Published online: 2020-05-18

Perylene Bisimide Cyclophanes: Structure–Property Relationships upon Variation of the Cavity Size

Jessica Rühe[a]
David Bialas[a]
Peter Spenst[a]
Ana-Maria Krause[b]
Frank Würthner*[a,b]

[a] Institut für Organische Chemie, Universität Würzburg, Am Hubland, 97074 Würzburg, Germany
[b] Center for Nanosystems Chemistry, Universität Würzburg, Theodor-Boveri-Weg, 97074 Würzburg, Germany
wuerthner@uni-wuerzburg.de

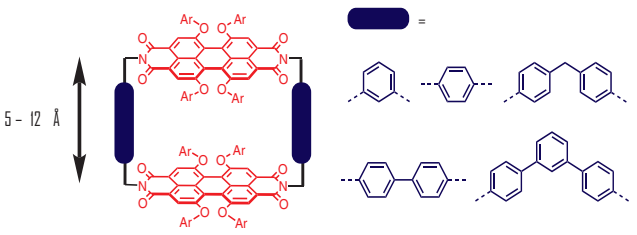

Received: 28.03.2020
Accepted after revision: 6.04.2020

DOI: 10.1055/s-0040-1709998; Art ID: 200009oa

Abstract Five cyclophanes composed of two perylene bisimide (PBI) dyes and various CH_2–arylene–CH_2 linker units were synthesized. PM6-D3H4 geometry-optimized structures and a single crystal for one of these cyclophanes reveal well-defined distances between the two coplanar PBI units in these cyclophanes, spanning the range from 5.0 to 12.5 Å. UV/vis absorption spectra reveal a redistribution of oscillator strength of the vibronic bands due to a H-type exciton coupling even for the cyclophane with the largest interchromophoric distance. A quantitative evaluation according to the Kasha–Spano theory affords exciton coupling strengths ranging from 64 cm^{-1} for the largest cyclophane up to 333 cm^{-1} for the smallest one and a surprisingly good fit to the cubic interchromophoric distance in the framework of the point-dipole approximation. Interchromophoric interaction is also noticed in fluorescence lifetimes that are significantly increased for all five cyclophanes as expected for H-coupled chromophores due to a decrease of the radiative rate. For the three largest cyclophanes with interchromophoric distances of >9 Å, fluorescence quantum yields remain high in chloroform (>88%), whilst for the smaller ones with interchromophoric distances <6 Å, additional nonradiative pathways lead to a pronounced fluorescence quenching.

Key words cyclophanes, exciton coupling, fluorescence, organic dyes

Introduction

Historically, the interest of chemists in cyclophanes was motivated by imparting strain in aromatic molecules such as [2.2]-paracyclophane,[1] which were described by Cram as "internally tortured molecules with inherent suicidal tendencies."[2] Later on, cyclophanes enjoyed increasing popularity in supramolecular chemistry with Stoddart's "blue box" cyclobis(paraquat-*p*-phenylene) as a most useful prototype due to its strong complexation of electron-rich aromatic guests such as dialkoxybenzenes,[3] which in combination with the cyclophane's redox activity enabled the control of motion in catenanes and rotaxanes by electrical stimuli.[4] However, despite the usefulness of cyclophane-based supramolecular host–guest complexes,[5] progress in the expansion of the applicable π-scaffolds was slow-going. For instance, it took until 2013 before Stoddart and co-workers reported on the ExBox, bearing just one additional *p*-phenylene unit, and its interesting complexation properties for a variety of larger aromatic π-scaffolds.[6]

More recently, cyclophanes demonstrated their usefulness for a variety of applications, which originate from the control of photofunctional properties.[7] In such systems, two dyes are positioned in space by a suitable linker that determines the distance and orientation between the dyes and by this means their electronic coupling. Indeed, whilst covalent dimers of a variety of chromophores have become favored systems since several decades for the elucidation of dye–dye interactions in the ground and excited states,[8] in earlier times often motivated by the special pair of chlorophylls in the photosynthetic reaction center,[9] dye-containing cyclophanes remained less investigated.[10] This is at first glance surprising because cyclophanes can offer a good control of orientation and distance of the chromophores in rather rigid geometries, which is ideal for deriving structure–property relationships and the supramolecular engineering of desirable functionality.[11] However, in particular for chromophores with low solubility and strong aggregation propensity, such as those given for perylene bisimide (PBI) dyes,[12] cyclophane synthesis can be quite challenging. Thus, it was only in 2015 that our group reported the first example for a PBI-based cyclophane (**3b**, Scheme 1) that was able to accommodate a variety of polycyclic aromatic hydrocarbons (PAHs) with high binding constants in its cavity.[13] What distinguished cyclophane **3b** from earlier PBI-based

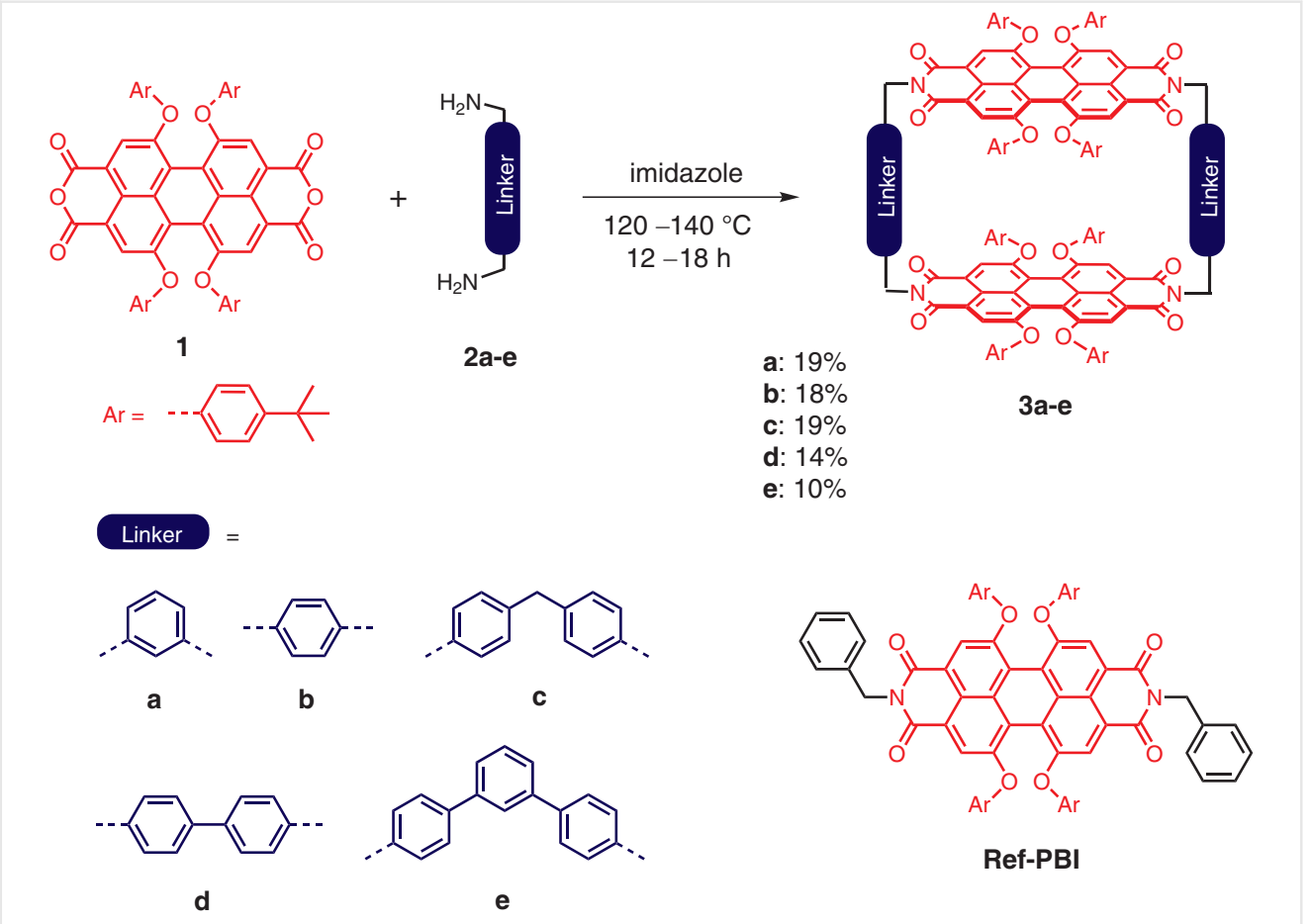

Scheme 1 Synthesis of PBI cyclophanes **3a–e** starting from 1,6,7,12-tetra (*tert*-butylphenoxy)-substituted perylene bisanhydride **1**[20] and the respective diamines **2a–e**. The synthesis of cyclophanes **3b–e** was performed in toluene to make use of the template effect. Also shown is the chemical structure of PBI chromophore **Ref-PBI**,[13a] which is used as a reference compound in this work.

cyclophanes[14] was the cavity size that was just ideal for the inclusion of PAH guest molecules such as perylene. However, due to the strong propensity of PBIs for aggregation,[15] it is not trivial to synthesize such cyclophanes and the number and type of phenoxy units in the bay area proved to be crucial. Thus, whilst a yield of 18% could be obtained for cyclophane **3b** bearing four *tert*-butylphenoxy substituents,[13] the yield in cyclophane synthesis dropped down to <1% for the related twofold *tert*-butylphenoxy-substituted PBIs[16] and could only raise up to 6% for those phenoxy groups bearing additional sterically demanding substituents in the *ortho*-position to prohibit PBI aggregation.[17] These results corroborate our hypothesis that the strong π–π-stacking propensity of PBIs countervails the efficient synthesis of PBI cyclophanes bearing open cavities and that the core distortion of the PBI π-scaffold imposed by four phenoxy units in the bay area[18] is highly supportive for the preparation of cyclophanes composed of PBIs. Based on this hypothesis, in this study we explore the synthesis of a series of tetraphenoxy-PBI cyclophanes **3a–e** bearing different linker units (Scheme 1) with the particular goal of modulating the size of the π-cavity and deriving relationships between dye–dye distances and functional properties, i.e. fluorescence and exciton coupling.

Results and Discussion

Synthesis

The synthetic procedure of five PBI cyclophanes is shown in Scheme 1. Cyclophanes bearing *meta*-xylene (**3a**)[19] and *para*-xylene (**3b**)[13] linker moieties are known and the synthesis of cyclophanes **3c–e** was performed under similar conditions. Accordingly, 1,6,7,12-tetra (*tert*-butylphenoxy)-substituted perylene bisanhydride **1**[20] was reacted with the respective diamines **2a–e** in imidazole. For the synthesis of cyclophane **3b**, a significant increase of the yield was

observed upon addition of toluene, which can be rationalized by a template effect.[13a] The addition of perylene, which showed a high binding constant for the encapsulation into cyclophane **3b** in former studies,[13a] did not lead to an increase of the yield. Hence, the synthesis of the cyclophanes was performed in toluene at low concentration to avoid the formation of undesired oligomers. Notably, for PBI cyclophane **3a**, bearing the shortest linker unit within the series (*meta*-xylene), no template effect was observed since the small cavity size (vide infra) prevents the enclosure of toluene molecules. Thus, **3a** was obtained in decent yields of 19% without the addition of toluene (Scheme 1). Cyclophanes **3a** and **3b** were purified by column chromatography, whereas for cyclophanes **3c–e** recycling gel permeation chromatography as well as preparative thin layer chromatography (in the case of **3c**) was applied to separate nondesired oligomeric side-products and larger macrocycles. For details on the synthetic procedures and characterization of the new PBI cyclophanes, see the Experimental Section.

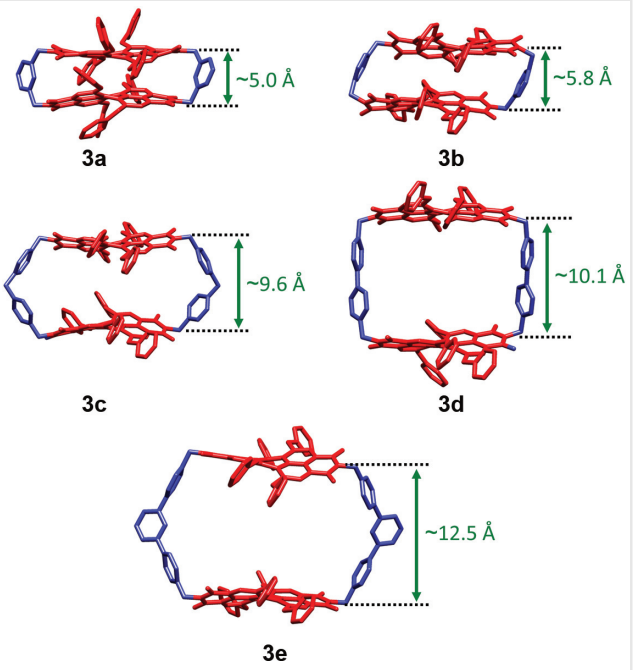

Figure 1 Geometry-optimized structures (PM6-D3H4)[21,23] of PBI cyclophanes **3a–e** with increasing size of the linker. Hydrogen atoms and butyl groups are omitted for clarity. The PBI chromophores and linker moieties are colored in red and blue, respectively.

Molecular Modeling

In order to gain insight into the interchromophoric distances within the cyclophanes, geometry optimizations have been performed. Toward this goal, the semiempirical Hamiltonian PM6[21] was used as implemented in the MOPAC program package.[22] In addition, the D3H4 correction[23] was employed to also account for dispersion interactions. The geometry-optimized structures of PBI cyclophanes **3a–e** are displayed in Figure 1. As expected, the cavity size increases with the length of the linker unit, ranging from 5.0 Å (**3a**) to 12.5 Å (**3e**). The *tert*-butylphenoxy groups in the bay position of the chromophores can cover a wide conformational space,[18a] which may lead to sterical encounters, thereby influencing the interchromophoric distances for the cyclophanes **3a–c** with shorter linker moieties. Therefore, the distances given in Figure 1 are defined as the distance between the CH_2 groups of the spacer units linked to the imide groups of the PBI chromophores, which should not be affected by the arrangement of the bay substituents.

Known for bay-substituted PBI dyes,[18a] the *tert*-butylphenoxy groups induce a twist of the naphthalene moieties of the perylene core leading to the presence of atropisomers, which can interconvert at room temperature.[24] Since we are mainly interested in the dimensions of the cavities and in order to reduce computational effort, we have only minimized the structure of the homochiral pair for each cyclophane, i.e., (*P,P*)-configuration. In this way, a torsional twist of ~27° between the two naphthalimide subunits of each PBI is obtained for all cyclophanes, which is in good agreement with the values found in the solid state for fourfold phenoxy-substituted PBIs.[18a] It is worth noting that different conformations other than the ones shown in Figure 1 are present in solution. However, the linker moieties ensure a quite fixed distance of the PBI chromophores. Hence, the results obtained from geometry optimizations indeed show that the chosen linker moieties are suitable to modulate the cavity size and to ensure diverse interchromophoric distances.

Single-Crystal X-Ray Structure

In general, PBIs bearing four phenoxy substituents in the bay area are conformationally very flexible and not easy to pack in an ordered fashion in the crystalline state. Therefore, only few crystal structures are available for these molecules.[25] For cyclophanes with large cavities, the situation is even more difficult as the crystal may collapse when the solvent diffuses out of the cavity. However, PBI cyclophane **3d** bearing biphenylene linker units crystallized rather easily. Accordingly, single crystals of **3d** suitable for X-ray diffraction analysis were obtained by slow diffusion of *n*-hexane into a solution of the cyclophane in chloroform. The molecule crystallizes in a $P\bar{1}$ point group with one cyclophane moiety in the unit cell. Hence, the cyclophane shows an inversion center. Furthermore, the two PBI moieties of the cyclophane are coplanar in the solid state (Figure 2a) and are not rotationally displaced as observed for many stacked PBI chromophores.[11] The distance between the carbon atoms of the CH_2 groups of

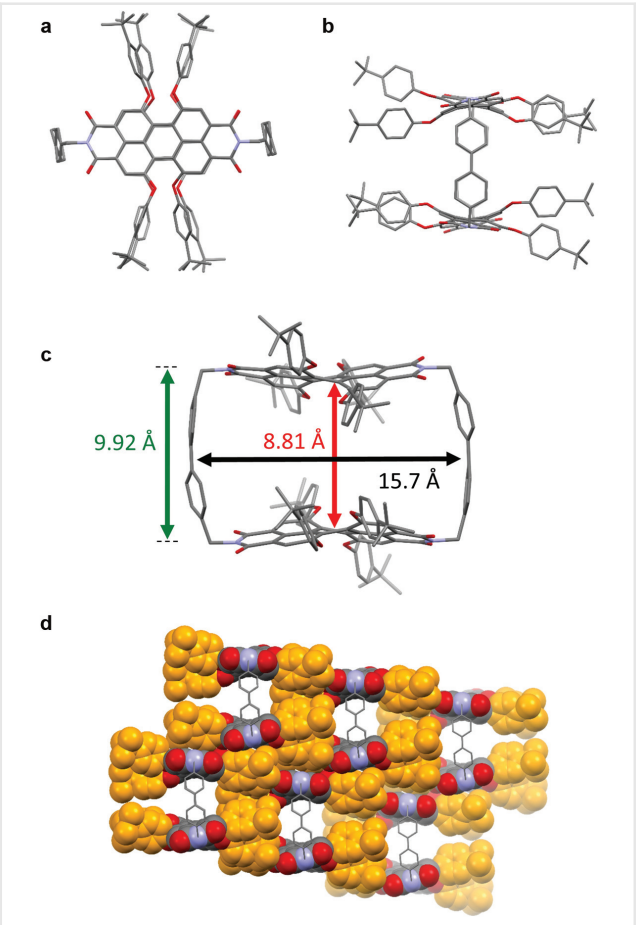

Figure 2 Molecular structure of cyclophane **3d** found in single crystals in (a) top view, (b) front, and (c) side view. (d) In addition, the packing arrangement in the crystal is shown in front view. Hydrogen atoms are omitted for clarity. Carbon, oxygen, and nitrogen atoms are colored in grey, red, and violet, respectively. In panel (d), the PBI chromophores and *tert*-butylphenoxy groups (highlighted in orange) are displayed in a space-filling model.

the linker is 9.92 Å, which is in good agreement with the value of 10.1 Å obtained from geometry optimizations (Figure 1). The median distance between the carbon atoms of the central ring of the PBI moieties is reduced to 8.81 Å (Figure 2c), caused by the slightly curved structure of the chromophores. The π-surfaces of the phenyl rings of the linker point towards the cavity with a distance of 15.7 Å.

The sterically demanding bay substituents point away from the cavity. Similar to other tetraphenoxy-substituted PBIs,[25] the symmetry is broken, i.e., the phenoxy groups are oriented in different conformations at the two opposing bay areas. In the crystal, the cavity is filled with a heavily disordered solvent (*n*-hexane), which was removed by the SQUEEZE routine in our crystallographic analysis.[26] Interestingly, the crystal structure exclusively shows the heterochiral (*P,M*)-configuration, which might be preferred to enable a nonchiral space group in the crystal. The angle of torsional twist of the PBI moiety that is induced by the bulky bay substituents is about 29°, which is similar to those of monomeric fourfold phenoxy-substituted PBIs[18a] and again in good agreement with the value obtained from molecular modeling of 27°. Furthermore, the packing of the cyclophanes reveals that there is no π–π stacking between adjacent cyclophanes (Figure 2d), which is probably due to the steric hindrance by the bulky bay substituents (highlighted in orange).

UV/Vis Absorption and Fluorescence Spectroscopy

Due to the fact that the transition dipole moment for the $S_0 \rightarrow S_1$ transition of PBIs is oriented along the long molecular axis,[11] these PBI cyclophanes with their exact linker-controlled distances constitute ideal systems to elucidate interchromophoric interactions. Accordingly, the optical properties of the PBI cyclophanes were studied via UV/vis absorption and fluorescence spectroscopy. The respective data in chloroform are summarized in Table 1 in comparison to a monomeric reference compound, **Ref-PBI**.[13a] The UV/vis absorption spectrum of **Ref-PBI** in chloroform shows

Table 1 Absorption and fluorescence data of cyclophanes **3a–e** and **Ref-PBI** in chloroform at 293 K (in addition, the exciton coupling strength *J* is given as estimated based on the absorption spectra)

	3a	**3b**[13a]	**3c**	**3d**	**3e**	**Ref-PBI**[13a]
λ_{abs} (A_{0-0})/nm	577	586	585	589	589	588
λ_{abs} (A_{0-1})/nm	541	547	546	549	548	547
A_{0-0}/A_{0-1}	1.12	1.25	1.45	1.48	1.56	1.66
ε_{max} (A_{0-0}) [M^{-1} cm^{-1}]	66000	60000	70400	60000	71100	41000
ε_{max} (A_{0-1}) [M^{-1} cm^{-1}]	59000	48000	48700	40400	45600	24700
λ_{em} [nm][a]	627	631	622	626	626	620
$\Delta\tilde{\nu}_{stokes}$ [cm^{-1}]	1382	1217	1017	1003	1003	878
Φ_{fl} [%][b]	9	21	88	93	94	97
τ_{fl} [ns], (ampl./%)[c]	10.0 (65) 0.72 (35)	12.5 (68) 0.55 (32)	8.2	7.8	7.2	6.5
k_{fl}[10^8 s^{-1}][d]	0.09	0.17	1.07	1.19	1.31	1.49
k_{nr} [10^8 s^{-1}][d]	0.91	0.63	0.14	0.09	0.08	0.05
J [cm^{-1}][e]	333	244	123	107	64	—

[a]The solutions were excited at the wavelength of the 0 – 1 absorption band.
[b]The fluorescence quantum yields were measured relative to *N,N'*-bis(2,6-diisopropylphenyl)-1,6,7,12-tetraphenoxy-3,4:9,10-perylene tetracarboxylic diimide ("Perylene Red")[27] as a reference at four different excitation wavelengths.
[c]For lifetime measurements a pulsed laser diode with a wavelength of 505.8 nm was used.
[d]Determined according to $k_{fl} = \Phi_{fl}/\tau_{fl}$ and $k_{nr} = 1/\tau_{fl} - k_{fl}$.
[e]Calculated based on Equation (1).

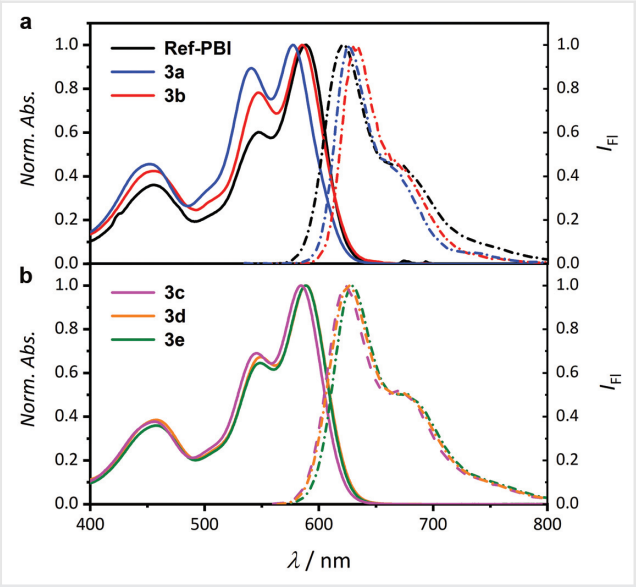

Figure 3 Normalized UV/vis absorption (solid lines, $c \approx 10^{-5}$ M) and fluorescence spectra (dash-dotted lines) of (a) **Ref-PBI** and PBI cyclophanes **3 a,b** as well as of (b) **3c–e** in chloroform at 293 K. For the detection of the fluorescence spectra, the samples were excited at the wavelength of the 0–1 absorption band.

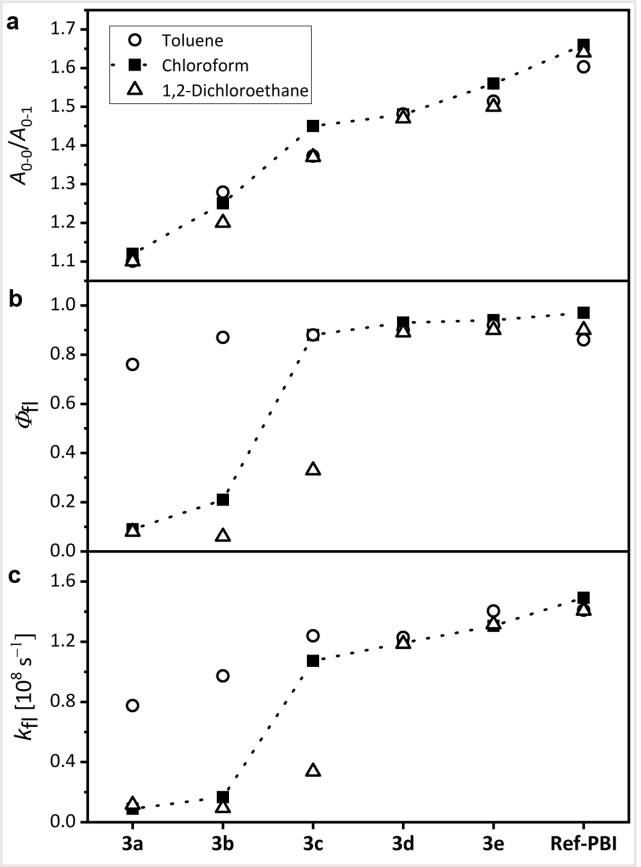

Figure 4 (a) Intensity ratio of the 0–0 and 0–1 absorption bands of PBI cyclophanes **3a–e** and **Ref-PBI** in solvents of different polarity. In addition, (b) the fluorescence quantum yield Φ_{fl} and (c) fluorescence rate constant k_{fl} are shown.

a typical pattern for PBIs with a pronounced vibronic fine structure (Figure 3a, black solid line). The main absorption band corresponding to the $S_0 \rightarrow S_1$ transition is observed at 588 nm with a vibronic progression (A_{0-1}) at 547 nm, whereas the absorption band at ~450 nm occurs from the $S_0 \rightarrow S_2$ transition.[27] In comparison to the monomeric reference dye, the absorption spectrum of cyclophane **3a** with the shortest linker unit shows a significant redistribution of oscillator strength of the vibronic bands (Figure 3a, blue solid line). Accordingly, a decrease in the ratio (A_{0-0}/A_{0-1}) of the intensity of the $0-0$ and $0-1$ bands from 1.66 for **Ref-PBI** to 1.12 for PBI cyclophane **3a** is observed (Figure 4a, filled squares). This is indicative of interchromophoric interaction between the chromophores in terms of exciton–vibrational coupling (H-type coupling).[28] For better comparison of the A_{0-0}/A_{0-1} ratios for the different cyclophanes, the spectra are normalized and shown in Figure 3 (for the spectra with extinction coefficients, see Figure S1 in the Supporting Information). In the case of cyclophane **3b** bearing a slightly larger interchromophoric distance, the ratio $A_{0-0}/A_{0-1} = 1.25$ is augmented (Figure 3a, red solid line) with respect to cyclophane **3a**, revealing a weaker exciton coupling. For cyclophanes **3c–e**, significantly larger A_{0-0}/A_{0-1} ratios are observed, ranging from 1.45 for cyclophane **3c** to 1.56 for cyclophane **3e** (Figures 3b and 4a). The latter value is only slightly lower than the one observed for **Ref-PBI**, indicating only a weak but still noticeable H-type coupling within the cyclophane **3e**. In the case of a π-stacked arrangement of the chromophores, we would expect a ratio of $A_{0-0}/A_{0-1} \approx 0.72$,[29] which is distinctly smaller than the ratios observed for the PBI cyclophanes **3a–e**. This suggests for all cyclophanes within this series that the cavity is open and a defined interchromophoric distance is present. Indeed, the ratio increases slightly within the series **3c–e** (Figure 4a), which is in accordance with the expected increase of interchromophoric distance according to the geometry-optimized structures (Figure 1) and therefore decrease of interaction. Furthermore, the ratio A_{0-0}/A_{0-1} is not significantly influenced by the polarity of the solvent (Figure 4a), revealing similar exciton coupling strength in the different solvents.

The fluorescence spectra of the cyclophanes in chloroform resemble the one of monomeric **Ref-PBI** (Figure 3, dash-dotted lines) with an increasing Stokes shift from 1,003 cm^{-1} (**3e**) to 1,382 cm^{-1} (**3a**) with decreasing length of the linker. This is in agreement with an augmented exciton coupling between the chromophores for shorter distances. Hence, a larger energetic splitting of the vibrational levels occurs that leads to an increased relaxation energy in the excited state.[28b] For a perfect

H-aggregate, the 0–0 fluorescence band is suppressed since the transition from the lowest excited state is forbidden.[28b] However, cyclophanes **3a–e** all show an intense 0–0 emission band, which can be caused by a rotational displacement of the chromophores,[30] thermal activation of higher allowed excited states,[31] and/or by disorder,[32] presumably arising from the conformational flexibility of the bay substituents. For cyclophanes **3c–e** also the fluorescence quantum yields remain high (88–94%), whilst the fluorescence quantum yields are significantly quenched for cyclophanes **3a** and **3b** (Table 1 and Figure 4b). As shown in previous work using time-resolved absorption spectroscopy, this decrease is not only caused by the H-type exciton coupling, but also by an additional relaxation pathway, i.e., symmetry-breaking charge separation, being favored for shorter interchromophoric distances.[13b,19b] This conclusion is supported by the observation that the fluorescence quantum yield is distinctly higher in solvents of lower polarity such as toluene (Figure 4b, open circles), in which the driving force for charge separation is reduced due to a less efficient stabilization of the charge-separated state. Notably, a significant drop of the fluorescence quantum yield is also observed for PBI cyclophane **3c** in the more polar solvent 1,2-dichloroethane (Figure 4b, open triangles), indicating a competing photoinduced symmetry-breaking charge separation also in the case of **3c** in this solvent.

We have also determined the fluorescence lifetime τ_{fl} to gain deeper insight into the excited-state properties of the coupled chromophores. Accordingly, compared to 6.5 ns for **Ref-PBI**, an increase of the lifetime from 7.2 ns (**3e**) to 10.0 ns (**3a**) with decreasing interchromophoric distance can be observed (Table 1). This increase can be attributed to the H-type coupling between the PBI chromophores. With decreasing interchromophoric distance within this series of cyclophanes, H-type coupling increases (vide infra), thereby reducing the oscillator strength for the radiative process and the fluorescence decay rates k_{fl} with respect to the single chromophore of **Ref-PBI** (Table 1 and Figure 4c). Together with the measured fluorescence quantum yields, we can also calculate the rate constants k_{nr} for the nonradiative decay. Hence, the nonradiative relaxation remains slow for **Ref-PBI** and the larger cyclophanes but becomes significantly faster at short interchromophoric distances (Table 1), in agreement with the observation of an effective additional charge separation process between PBI chromophores lying in close spatial proximity.[13b,19b]

It is worth noting that for the smallest cyclophanes **3a** and **3b**, a biexponential fit had to be applied in order to describe the fluorescence decay, which results in a long- and a short-living component. This can be rationalized by the population of different conformations in the ground state enforced by the flexible phenoxy groups,[18a,25] showing distinctly different fluorescence lifetimes upon excitation.

Theoretical Investigations

Exciton–vibrational coupling in PBI aggregates results in a redistribution of oscillator strength of the vibronic bands.[28,30] The vibronic contribution arises from the coupling of the electronic $S_0 \rightarrow S_1$ transition to the C–C stretching mode of the PBI core, which causes the pronounced vibronic progression as observed in the absorption spectrum of the monomeric PBI chromophore **Ref-PBI** (Figure 3a, black line). For H-type-coupled dye aggregates, a decrease of the A_{0-0}/A_{0-1} ratio is observed, the magnitude of which depends on the exciton coupling strength. Hence, it is possible to determine the coupling strength based on the changes of the intensity of the A_{0-0} band and an increase of the intensity of the A_{0-1} band. In the weak coupling regime (i.e., exciton coupling is weaker than vibronic coupling), the ratio of the band intensities for two coupled oscillators in our cyclophane architecture is given by:[30]

$$\frac{I_A^{(0-0)}}{I_A^{(0-1)}} = \frac{1}{\lambda^2}\left[\frac{1 - G(0,\lambda^2)\, e^{-\lambda^2} J/\omega_0}{1 - G(1,\lambda^2)\, e^{-\lambda^2} J/\omega_0}\right]^2 \quad (1)$$

where ω_0 is the vibrational frequency and λ^2 the Huang–Rhys factor, which determine the strength of the vibronic coupling. In addition, $G(\nu_t, \lambda^2)$ is the vibrational function and J the exciton coupling strength. The Huang–Rhys factor λ^2 and vibrational frequency ω_0 can be estimated from the intensity ratio and energetic difference of the 0–1 and 0–0 absorption bands[30] of the monomeric chromophore of **Ref-PBI**, respectively (for details see the Supporting Information). In this way, a value of $\lambda^2 = 0.59$ is obtained, in accordance with previously reported results for PBI chromophores.[30,33] The resulting exciton coupling strengths are listed in Table 1. Hence, PBI cyclophane **3a** with the shortest interchromophoric distance exhibits the strongest coupling ($J = 333$ cm^{-1}), while the weakest coupling ($J = 64$ cm^{-1}) is indeed present for cyclophane **3e** with the largest cavity size. Notably, these values are all significantly smaller than the vibronic coupling strength ($\lambda^2\omega_0 = 787$ cm^{-1}) in PBI cyclophanes **3a–e** and thereby justify the application of Equation (1). Furthermore, the calculated exciton coupling strengths in the PBI cyclophanes **3a–e** are distinctly smaller than the value determined for a π-stacked cyclophane bearing two tetraphenoxy-substituted PBI chromophores (500 cm^{-1}) at a short interchromophoric distance of ~3.8 Å.[34] Therefore, it is reasonable to assume an open cavity for all PBI cyclophanes with significantly larger distances. Figure 5 shows the exciton coupling strength as a function of the distance r between the chromophores within the cyclophanes (filled squares). In addition, the results obtained by applying the point-dipole approximation (green line) are shown, which describe the exciton coupling as the Coulomb interaction between the transition dipole moments μ_{eg} of the chromophores:[35]

$$J = \frac{\mu_{eg}^2}{4\pi\varepsilon_0\varepsilon_r r^3} \quad (2)$$

Equation (2) assumes a perfect H-aggregate without any rotational displacement of the transition dipole moments. ε_0 and ε_r are the vacuum permittivity and the relative permittivity of the solvent, respectively, while r represents the center-to-center distance of the transition dipole moments of the chromophores. Hence, the coupling strength should scale with $1/r^3$, which is in good agreement with the trend observed for PBI cyclophanes **3a–e** (Figure 5). We have used a value of $\mu_{eg} = 6.82$ D as estimated from the absorption spectrum of **Ref-PBI** (for details see Supporting Information). The results are rather striking since the applicability of the point-dipole approximation has been questioned for smaller interchromophoric distances in many previous studies in the last 50 years.[36]

In Equation (2), we have used the permittivity of chloroform ($\varepsilon_r = 4.81$). This might be an oversimplification, because it is uncertain if an inclusion of the solvent molecules into the cavity of the smaller cyclophanes **3a,b** occurs. Therefore, in the future we would like to shine light on this surprising outcome. In addition, a rotational twist motion of the chromophores along the axis defined by the centers of the PBI moieties can occur in solution. This will influence the exciton coupling strength, and thus, have an impact on the redistribution of oscillator strengths of the vibronic bands in the UV/vis absorption spectrum.[30] Nonetheless, our studies reveal that the increasing exciton coupling with decreasing cavity size significantly affects the optical properties of the cyclophanes.

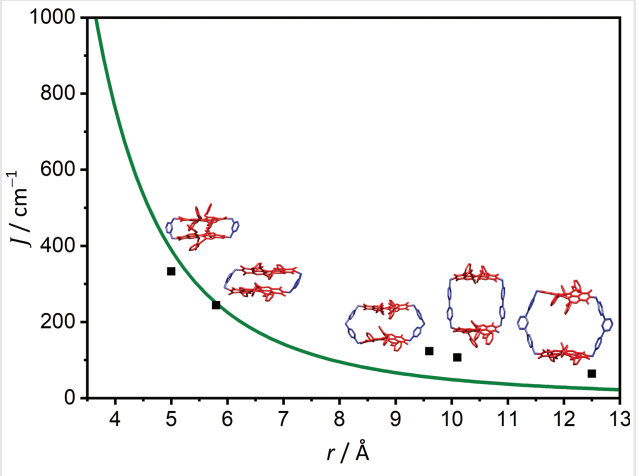

Figure 5 Exciton coupling strength J as a function of the interchromophoric distance r within the series of PBI cyclophanes **3a–e**. The filled squares represent the values determined based on Equation (1) using the absorption spectra in chloroform. In addition, the results obtained by applying the point-dipole approximation according to Equation (2) are shown as a green line.

Conclusions

In conclusion, we have reported a series of cyclophane architectures bearing two PBI dyes at defined interchromophoric distances between 5.0 and 12.5 Å. Different from other covalently tethered dye dimers,[8] the geometry in the cyclophanes **3a–e** is exactly defined with regard to the interchromophoric distance and the coplanar orientation of the dyes' transition dipole moments. This allowed us to derive relationships between structure and optical properties (absorption, fluorescence) at an unrivaled accuracy. Thus, a monotonous increase in H-type exciton coupling strength from 64 to 333 cm^{-1} was observed with decreasing interchromophoric distance, leading to a decrease of the A_{0-0}/A_{0-1} intensity ratio of the vibronic bands in absorption spectra, a decrease in fluorescence quantum yields and radiative rates, and an increasing Stokes shift. Whilst all of these observations are in accordance with Kasha's molecular exciton coupling theory and recent extensions by Spano, for the cyclophanes with the shortest linker units additional nonradiative decay processes were deduced from our analysis, which can be related to energetically favored symmetry-breaking charge separation processes.[13b,19b] Accordingly, our results demonstrate that cyclophane architectures are perfectly suited to derive unambiguous insights into interchromophoric interactions, because they allow positioning dyes at well-defined positions in space.

Experimental Section

Procedures

Chemicals and solvents were purchased from commercial suppliers (abcr GmbH, Alfa Aesar, Grüssing GmbH, Acros Organics, Fluorochem Ltd, Merck, Sigma-Aldrich, TCI Chemicals, and Fisher Scientific). Dry solvents were obtained from the purification system PS-M6-6/7-En from *Inert Technologies*.

Column chromatography was performed using standard glass columns of different sizes, packed with silica gel with a particle size of 40–63 µM purchased from *Macherey-Nagel* as a stationary phase. All solvents used for the column chromatography were distilled before use. Preparative thin-layer chromatography (TLC) was carried out with ALUGRAM® Xtra SIL G/UV254 (layer thickness: 0.2 mm) TLC plates, purchased from *Macherey-Nagel.*

For gel permeation chromatography (GPC) purification, the preparative recycling GPC system LaboACE from Japan

Analytical Industry Co., Ltd. (JAI) with PLgel Prep columns from Agilent Technologies (eluent: $CHCl_3$/methanol 9:1) was used.

All electrospray ionization (ESI) mass spectra were recorded on a micrOTOF focus spectrometer from *Bruker Daltonics GmbH*.

The melting points were determined using a polarization microscope BX41 from *Olympus* equipped with a TP-94 temperature regulation system from *Linkam Scientific* and are uncorrected.

All ^{1}H NMR and ^{13}C NMR spectra were recorded with an Avance III HD 400 spectrometer from *Bruker* operating at 400 MHz (^{1}H) or 101 MHz (^{13}C) or on a DMX 600 from *Bruker* operating at 600 MHz (^{1}H) or 151 MHz (^{13}C). Chemical shifts are listed in parts per million and are reported using the residual solvent signal as calibration standard. The multiplicities for proton signals are abbreviated as s, d, dd, t, and m for singlet, doublet, doublet of doublets, triplet, and multiplet.

UV-vis absorption spectra were measured with a V-770 spectrophotometer (*Jasco*) equipped with a JASCO PAC-743R Auto Peltier 6/8-cell changer system for the temperature control. Standard quartz glass cuvettes (*Hellma*) and spectroscopy-grade chloroform, toluene, and 1,2-dichloroethane were used.

Fluorescence studies were carried out on an FLS980 spectrometer from *Edinburgh Instruments*. Standard quartz glass cuvettes from *Hellma* with a path length of 1 cm and spectroscopy-grade chloroform, toluene, and 1,2-dichloroethane were used. The fluorescence quantum yields (Φ_{fl}) were determined as average values at four different excitation wavelengths (520, 525, 530, and 535 nm) using *N*,*N*'-(2,6-di-iso-propylphenyl)-1,6,7,12-tetraphenoxy-perylene-3,4:9,10-tetracarboxylic acid bisimide (Φ_{fl} = 96% in chloroform)[26] as standard under highly diluted (OD$\leq$ 0.05) and magic angle (54.7°) conditions. The fluorescence lifetimes were determined via time correlated single photon counting (TCSPC) using an EPL picosecond pulsed diode laser (λ_{fl} = 505.8 nm) with a pulse width of 141.7 ps with an FLS980-D2D2-ST spectrometer (Edinburgh Instruments Ltd., UK) under magic-angle conditions (54.7°). The fitting of the data was carried out using the Tail-Fit routine supplied by Edinburgh Instruments Ltd., Inc. For lifetimes <3 ns, the reconvolution fit routine supplied by Edinburgh Instruments Ltd., Inc. was used, taking the instrument response function into consideration.

X-Ray Structure Analysis

Single-crystal X-ray diffraction data for **3d** were collected at 100 K on a Bruker D8 Quest Kappa diffractometer with a Photon100 CMOS detector and multilayered mirror monochromated CuK_α radiation. The structure was solved using direct methods, expanded with Fourier techniques, and refined with the Shelx software package.[37] All non-hydrogen atoms were refined anisotropically. Hydrogen atoms were included in the structure factor calculation on geometrically idealized positions. The refinement showed solvent molecules in the cavity of the cyclophanes, which could not be modeled satisfactorily. Therefore, the SQUEEZE routine of PLATON was used to remove the respective electron density.[26] The remaining structure could be refined adequately. Crystal data for **3d** ($C_{156}H_{136}N_4O_{16}$ + solvent): M_r = 2322.68, red block, 0.096 × 0.062 × 0.056 mm^3, triclinic space group $P\bar{1}$, a = 15.1230(10) Å, α = 102.166(3)°, b = 16.7031(11) Å, β = 100.936(3)°, c = 16.5230(4) Å, γ = 69.0340(10)°, V = 3712.3(4) Å^3, Z = 2, ρ (calcd.) = 1.039 g cm^{-3}, μ = 0.530 mm^{-1}, $F(000)$ = 1228, $GooF(F^2)$ = 1.074, R_1 = 0.0478, wR^2 = 0.1302 for $I > 2\sigma(I)$, R_1 = 0.0583, wR^2 = 0.1374 for all the data, 14534 unique reflections ($\theta \leq$ 72.396°) with a completeness of 99.8% and 818 parameters, 6 restraints. Crystallographic data have been deposited with the Cambridge Crystallographic Data Centre as supplementary publication no. CCDC 1992950. This data can be obtained free of charge from the Cambridge Crystallographic Data Centre via www.ccdc.cam.ac.uk/data_request/cif.

Synthesis

The precursors *meta*- and *para*-xylylenediamine were commercially available, whereas 4,4'-bis(aminomethyl)biphenyl,[38] bis(4-aminomethylphenyl)-methane,[39] and [1,1′:3′,1″-terphenyl]-4,4″-dimethanamine[40] were prepared according to literature-known procedures. The synthesis of 1,6,7,12-tetrakis-4-*tert*-butylphenoxyperylene-3,4:9,10-tetracarboxylic acid bisanhydride (**1**) is also described in the literature.[20]

PBI Cyclophane (3a)

Perylene bisanhydride **1** (100 mg, 102 µmol, 1.0 eq.), *meta*-xylylenediamine (14.0 mg, 102 µmol, 1.0 eq.), and imidazole (2.0 g) were stirred under a nitrogen atmosphere for 12 h at 140 °C. After cooling to room temperature, 2N HCl_{aq} (200 mL) was added and the solution subsequently extracted with dichloromethane. The organic solvent was removed under reduced pressure and the crude product purified by column chromatography (silica gel, DCM) to obtain pure cyclophane **3a** as a red solid (21.0 mg, 9.68 µmol, 19%). M.p. > 300 °C. ^{1}H-NMR ($CDCl_3$, 600 MHz, 295 K): δ [ppm] = 8.14 (s, 4 H), 7.99 (s, 4 H), 7.55 (m, 2 H), 7.47 (dd, ^4J (H,H) = 1.4 Hz, ^3J (H,H) = 7.7 Hz, 4 H), 7.33 (d, ^3J (H,H) = 8.6 Hz, 8 H), 7.20 (t, ^3J (H, H) = 7.7 Hz, 2 H), 7.10 (d, ^3J (H,H) = 8.6 Hz, 8 H), 7.01 (d, ^3J (H,H) = 8.6 Hz, 8 H), 6.35 (d, ^3J (H,H) = 8.6 Hz, 8 H), 5.61 (d, ^3J (H,H) = 13.5 Hz, 4 H), 4.81 (d, ^3J (H,H) = 13.5 Hz, 8 H),

1.38 (s, 36 H), 1.25 (s, 36 H). ^{13}C-NMR ($CDCl_3$, 151 MHz, 295 K): δ [ppm] = 163.1, 156.5, 154.2, 153.9, 152.4 147.5, 147.0, 137.4, 132.9, 131.4, 130.7, 127.8, 127.0, 126.8, 123.0, 122.5, 121.7, 121.5, 119.6, 119.5, 119.1, 118.3, 43.2, 34.6, 34.5, 31.7, 31.5. Two signals were not observed due to overlap with other signals. HRMS (ESI, positive mode): m/z = 2169.94021 $[M + H]^+$ (calcd. for $C_{144}H_{129}N_4O_{16}^+$: 2169.93981). UV/vis ($CHCl_3$, c = 50 µM): λ_{abs} [nm] (ε_{max}, [M^{-1} cm^{-1}]) = 577 (66000), 541 (59000), 451 (30100). Fluorescence ($CHCl_3$): λ_{em} [nm](λ_{ex} [nm]) = 627 (530), PLQY ($CHCl_3$): Φ_{fl} [%] = 9.

PBI Cyclophane (3c)

Perylene bisanhydride **1** (90.0 mg, 91.4 µmol, 1.0 eq.), bis(4-aminomethylphenyl)methane (20.7 mg, 91.4 µmol, 1.0 eq.), and imidazole (1.35 g) were suspended in dry toluene (250 mL). The reaction mixture was stirred at 120 °C for 18 h. The mixture was allowed to cool down to room temperature and the solvent was removed under reduced pressure. The residue was dissolved in chloroform (50 mL) and washed with 1N $HCl_{aq.}$ (2 × 100 mL) and water (100 mL). The organic phase was dried over $MgSO_4$ and the solvent was evaporated. The crude product was purified by filtration through a silica plug (DCM) and recycling GPC (chloroform/MeOH 9:1) to give **3c** as a red solid (20.4 mg, 8.68 µmol, 19%). M.p. > 300 °C. ^{1}H-NMR (1,1,2,2-$C_2D_2Cl_4$, 400 MHz, 390 K): δ [ppm] = 8.18 (s, 8H), 7.36 (d, ^3J = 7.8 Hz, 8H), 7.23 (d, ^3J = 8.6 Hz, 16H), 7.09 (d, ^3J = 7.8 Hz, 8H), 6.83 (d, ^3J = 8.6 Hz, 16H), 5.24 (s, 8H), 3.93 (s, 4H), 1.34 (s, 72H). ^{13}C-NMR (1,1,2,2-$C_2D_2Cl_4$, 151 MHz, 360 K): δ [ppm] = 163.1, 155.7, 152.6, 147.3, 139.8, 134.6 132.7, 128.8, 128.7, 126.3, 122.1, 120.5, 119.7, 119.2, 119.1, 43.2, 34.1, 31.3, 29.5. HRMS (ESI, positive mode): m/z = 1197.49862 $[M + Na_2]^{2+}$ (calcd. for $C_{158}H_{140}N_4Na_20_{16}^{2+}$: m/z = 1197.50244). UV/vis ($CHCl_3$, c = 10 µM): λ_{abs} [nm] (ε_{max}, [M^{-1} cm^{-1}]) = 585 (70400), 546 (48700), 458 (25600). Fluorescence ($CHCl_3$): λ_{em} [nm](λ_{ex} [nm]) = 622 (546). PLQY ($CHCl_3$): Φ_{fl} [%] = 88.

PBI Cyclophane (3d)

Perylene bisanhydride **1** (90.0 mg, 91.4 µmol, 1.0 eq.), 4,4'-bis(aminomethyl)biphenyl (18.5 mg, 91.4 µmol, 1.0 eq.), and imidazole (1.35 g) were suspended in dry toluene (250 mL). The reaction mixture was stirred at 120 °C for 18 h. The mixture was allowed to cool down to room temperature and the solvent was removed under reduced pressure. The residue was dissolved in chloroform (50 mL) and washed with 1N HCl_{aq} (2 × 100 mL) and water (100 mL). The organic phase was dried over $MgSO_4$ and the solvent was evaporated. The crude product was purified by filtration through a silica plug (DCM), recycling GPC (chloroform/MeOH 9:1), and preparative TLC (silica gel, DCM/cyclohexane 2:1) to give **3d** as a red solid (15.3 mg, 6.59 mmol, 14%). M.p. > 300 °C. ^{1}H-NMR (1,1,2,2-$C_2D_2Cl_4$, 400 MHz, 360 K): δ [ppm] = 8.17 (s, 8H), 7.48 (d, ^3J = 8.4 Hz, 8H), 7.41 (d, ^3J = 8.4 Hz, 8H), 7.25 (d, ^3J = 8.7 Hz, 16H), 6.82 (d, ^3J = 8.7 Hz, 16H), 5.36 (s, 8H), 1.35 (s, 72H). ^{13}C-NMR (1,1,2,2-$C_2D_2Cl_4$, 151 MHz, 352 K): δ [ppm] = 162.8, 155.6, 152.7, 147.3, 139.3, 136.5, 132.5, 129.6, 126.5, 126.4, 120.4, 120.2, 119.9, 119.2,119.0, 42.7, 34.1, 31.3. HRMS (ESI, positive mode): m/z = 2343.97555 $[M + Na]^+$ (calcd. for $C_{156}H_{136}N_4Na0_{16}^+$: m/z = 2343.98435). UV/vis ($CHCl_3$, c = 10 µM): λ_{abs} [nm] (ε_{max}, [M^{-1} cm^{-1}]) = 589 (60000), 549 (40400), 458 (23100). Fluorescence ($CHCl_3$): λ_{em} [nm] (λ_{ex} [nm]) = 626 (549). PLQY ($CHCl_3$): Φ_{fl} [%] = 93.

PBI Cyclophane (3e)

Perylene bisanhydride **1** (80.0 mg, 81.2 µmol, 1.0 eq.), [1,1':3',1''-terphenyl]-4,4''-dimethanamine (23.4 mg, 81.2 µmol, 1.0 eq.), and imidazole (1.35 g) were suspended in dry toluene (250 mL). The reaction mixture was stirred at 120 °C for 18 h. Subsequently, the mixture was allowed to cool down to room temperature and the solvent was removed under reduced pressure. The residue was dissolved in chloroform (50 mL) and washed with 1N $HCl_{aq.}$ (2 × 100 mL) and water (100 mL). The organic phase was dried over $MgSO_4$ and the solvent was evaporated. The crude product was purified by filtration through a silica plug (DCM) and recycling GPC (chloroform/MeOH, 9:1) to give **3e** as a red solid (10.2 mg, 4.12 µmol, 10%). M.p. > 300 °C. ^{1}H-NMR ($CDCl_3$, 400 MHz, 295 K): δ [ppm] = 8.23 (s, 8H), 7.55–7.42 (m, 24H), 7.19 (d, ^3J = 8.8 Hz, 16H), 6.78 (d, ^3J = 8.8 Hz, 16H), 5.34 (s, 8H, CH_2), 1.26 (s, 72H). ^{13}C-NMR ($CDCl_3$, 101 MHz, 295 K): δ [ppm] = 163.6, 156.2, 152.8, 147.5, 141.5, 140.5, 136.3, 133.0, 129.2, 128.9, 127.5, 126.8, 126.3, 125.9, 122.4, 120.7, 120.1, 119.6, 119.5, 43.6, 34.5, 31.6. HRMS (ESI, positive mode): m/z = 1259.51616 $[M + Na_2]^{2+}$ (calcd. for $C_{168}H_{144}N_4Na_20_{16}^{2+}$: 1259.51809). UV/vis ($CHCl_3$, c = 10 µM): λ_{abs} [nm] (ε_{max}, [M^{-1} cm^{-1}]) = 589 (71100), 548 (45600),457 (26700). Fluorescence ($CHCl_3$): λ_{em} [nm](λ_{ex} [nm]) = 626 (548). PLQY ($CHCl_3$): Φ_{fl} [%] = 94.

Funding Information

The authors are grateful for financial support from the Deutsche Forschungsgemeinschaft (DFG) within the research training school GRK 2112 on "Molecular Biradicals" at the University of Würzburg.

Supporting Information

Supporting information for this article is available online at https://doi.org/10.1055/s-0040-1709998.

References

(1) Steinberg, H.; Cram, D. J. *J. Am. Chem. Soc.* **1952**, *74*, 5388.
(2) Cram, D. J.; Cram, J. M. *Acc. Chem. Res.* **1971**, *4*, 204.
(3) Odell, B.; Reddington, M. V.; Slawin, A. M. Z.; Spencer, N.; Stoddart, J. F.; Williams, D. J. *Angew. Chem. Int. Ed.* **1988**, *27*, 1547.
(4) Stoddart, J. F. *Angew. Chem. Int. Ed.* **2017**, *56*, 11094.
(5) (a) Diederich, F. *Angew. Chem. Int. Ed.* **1988**, *27*, 362. (b) Liu, Z.; Nalluri, S. K. M.; Stoddart, J. F. *Chem. Soc. Rev.* **2017**, *46*, 2459.
(6) (a) Barnes, J. C.; Juríček, M.; Strutt, N. L.; Frasconi, M.; Sampath, S.; Giesener, M. A.; McGrier, P. L.; Bruns, C. J.; Stern, C. L.; Sarjeant, A. A.; Stoddart, J. F. *J. Am. Chem. Soc.* **2013**, *135*, 183. (b) Dale, E. J.; Vermeulen, N. A.; Juríček, M.; Barnes, J. C.; Young, R. M.; Wasielewski, M. R.; Stoddart, J. F. *Acc. Chem. Res.* **2016**, *49*, 262.
(7) Spenst, P.; Würthner, F. *J. Photochem. Photobiol., A* **2017**, *31*, 114.
(8) (a) Giaimo, J. M.; Gusev, A. V.; Wasielewski, M. R. *J. Am. Chem Soc.* **2002**, *124*, 8530. (b) Vauthey, E. *ChemPhysChem* **2012**, *13*, 2001. (c) Bartynski, A. N.; Gruber, M.; Das, S.; Rangan, S.; Mollinger, S.; Trinh, C.; Bradforth, S. E.; Vandewal, K.; Salleo, A.; Bartynski, R. A.; Bruetting, W.; Thompson, M. E. *J. Am. Chem. Soc.* **2015**, *137*, 5397. (d) Bialas, D.; Kirchner, E.; Würthner, F. *Chem. Commun.* **2016**, *52*, 3777. (e) Sung, J.; Nowak-Król, A.; Schlosser, F.; Fimmel, B.; Kim, W.; Kim, D.; Würthner, F. *J. Am. Chem. Soc.* **2016**, *138*, 9029. (f) Hetzer, C.; Guldi, D. M.; Tykwinski, R. R. *Chem. Eur. J.* **2018**, *24*, 8245. (g) Papadopoulos, I.; Zirzlmeier, J.; Hetzer, C.; Bae, Y. J.; Krzyaniak, M. D.; Wasielewski, M. R.; Clark, T.; Tykwinski, R. R.; Guldi, D. M. *J. Am. Chem. Soc.* **2019**, *141*, 6191.
(9) (a) Wasielewski, M. R. *Chem. Rev.* **1992**, *92*, 435. (b) Maruyama, K.; Osuka, A.; Mataga, N. *Pure Appl. Chem.* **1994**, *66*, 867.
(10) (a) Keshri, S. K.; Takai, A.; Ishizuka, T.; Kojima, T.; Takeuchi, M. *Angew. Chem. Int. Ed.* **2020**, *59*, 5254. (b) Adinarayana, B.; Kato, K.; Shimizu, D.; Tanaka, T.; Furukawa, K.; Osuka, A. *Angew. Chem. Int. Ed.* **2020**, *59*, 4320. (c) Zwick, P.; Weiland, K. J.; Malinčík, J.; Stefani, D.; Häussinger, D.; van der Zant, H. S. J.; Dulić, D.; Mayor, M. *J. Org. Chem.* **2020**, *85*, 118. (d) Nozawa, R.; Kim, J.; Oh, J.; Lamping, A.; Wang, Y. M.; Shimizu, S.; Hisaki, I.; Kowalczyk, T.; Fliegl, H.; Kim, D.; Shinokubo, H. *Nat. Commun.* **2019**, *10*, 3576.
(11) Würthner, F.; Saha-Möller, C. R.; Fimmel, B.; Ogi, S.; Leowanawat, P.; Schmidt, D. *Chem. Rev.* **2016**, *116*, 962.
(12) Chen, Z.; Lohr, A.; Saha-Möller, C. R.; Würthner, F. *Chem. Soc. Rev.* **2009**, *38*, 564.
(13) (a) Spenst, P.; Würthner, F. *Angew. Chem. Int. Ed.* **2015**, *54*, 10165. (b) Spenst, P.; Young, R. M.; Wasielewski, M. R.; Würthner, F. *Chem. Sci.* **2016**, *7*, 5428.
(14) (a) Langhals, H.; Ismael, R. *Eur. J. Org. Chem.* **1998**, 1915. (b) Feng, J.; Zhang, Y.; Zhao, C.; Lamping, A.; Wang, Y. M.; Shimizu, S.; Hisaki, I.; Kowalczyk, T.; Fliegl, H.; Kim, D.; Shinokubo, H. *Chem. Eur. J.* **2008**, *14*, 7000. (c) Schlosser, F.; Moos, M.; Lambert, C.; Würthner, F. *Adv. Mater.* **2013**, *25*, 410. (d) Ball, M.; Zhong, Y.; Fowler, B.; Zhang, B.; Li, P.; Etkin, G.; Paley, D. W.; Decatur, J.; Dalsania, A. K.; Li, H.; Xiao, S.; Ng, F.; Steigerwald, M. L.; Nuckolls, C. *J. Am. Chem. Soc.* **2016**, *138*, 12861.
(15) Chen, Z.; Fimmel, B.; Würthner, F. *Org. Biomol. Chem.* **2012**, *10*, 5845.
(16) Sieblist, A. Bachelor thesis. Universität Würzburg; **2014**.
(17) Spenst, P.; Sieblist, A.; Würthner, F. *Chem. Eur. J.* **2017**, *23*, 1667.
(18) (a) Würthner, F. *Pure Appl. Chem.* **2006**, *78*, 2341. (b) Nowak-Król, A.; Würthner, F. *Org. Chem. Front.* **2019**, *6*, 1272.
(19) (a) Spenst, P. PhD thesis. Universität Würzburg; **2016**. (b) Schultz, J. D.; Coleman, A. F.; Mandal, A.; Shin, J. Y.; Ratner, M. A.; Young, R. M.; Wasielewski, M. R. *J. Phys. Chem. Lett.* **2019**, *10*, 7498.
(20) Würthner, F.; Thalacker, C.; Sautter, A.; Schärtl, W.; Ibach, W.; Hollricher, O. *Chem. Eur. J.* **2000**, *6*, 3871.
(21) Stewart, J. J. P. J. *J. Mol. Model.* **2007**, *13*, 1173.
(22) (a) MOPAC2012. Stewart, J. J. P. Stewart Computational Chemistry, Version 14.045, web: http://OpenMOPAC.net. (b) Maia, J. D. C.; Urquiza Carvalho, G. A.; Mangueira, C. P. Jr; Santana, S. R.; Cabral, L. A. F.; Rocha, G. B. *J. Chem. Theory Comput.* **2012**, *8*, 3072.
(23) Řezáč, J.; Hobza, P. *J. Chem. Theory Comput.* **2012**, *8*, 141.
(24) Osswald, P.; Würthner, F. *J. Am. Chem. Soc.* **2007**, *129*, 14319.
(25) (a) Osswald, P.; Leusser, D.; Stalke, D.; Würthner, F. *Angew. Chem. Int. Ed.* **2005**, *44*, 250. (b) Hippius, C.; van Stokkum, I. H. M.; Zangrando, E.; Williams, R. M.; Wykes, M.; Beljonne, D.; Würthner, F. *J. Phys. Chem.* **2008**, *112*, 14626.
(26) Spek, A. L. *Acta Crystallogr. A* **1990**, *46*, C34.
(27) (a) Seybold, G.; Wagenblast, G. *Dyes Pigm.* **1989**, *11*, 303. (b) Gvishi, R.; Reisfeld, R.; Burshtein, Z. *Chem. Phys. Lett.* **1993**, *213*, 338.
(28) (a) Seibt, J.; Winkler, T.; Renziehausen, K.; Dehm, V.; Würthner, F.; Meyer, H. D.; Engel, V. *J. Phys. Chem. A* **2009**, *113*, 13475. (b) Spano, F. C. *Acc. Chem. Res.* **2010**, *43*, 429.
(29) Schlosser, F.; Moos, M.; Lambert, C.; Würthner, F. *Adv. Mater.* **2013**, *25*, 410.
(30) Kistler, K. A.; Pochas, C. M.; Yamagata, H.; Matsika, S.; Spano, F. C. *J. Phys. Chem. B* **2012**, *116*, 77.
(31) Oleson, A.; Zhu, T.; Dunn, I. S.; Bialas, D.; Bai, Y.; Zhang, W.; Dai, M.; Reichman, D. R.; Tempelaar, R.; Huang, L.; Spano, F. C. *J. Phys. Chem. C* **2019**, *123*, 20567.
(32) Hestand, N. J.; Spano, F. C. *Chem. Rev.* **2018**, *118*, 7069.
(33) Kaufmann, C.; Bialas, D.; Stolte, M.; Würthner, F. *J. Am. Chem. Soc.* **2018**, *140*, 9986.
(34) Bialas, D.; Brüning, C.; Schlosser, F.; Fimmel, B.; Thein, J.; Engel, V.; Würthner, F. *Chem. Eur. J.* **2016**, *22*, 15011.
(35) Kasha, M.; Rawls, H. R.; El-Bayoumi, M. A. *Pure Appl. Chem.* **1965**, *11*, 371.
(36) (a) Czikklely, V.; Forsterling, H. D.; Kuhn, H. *Chem. Phys. Lett.* **1970**, *6*, 207. (b) Beljonne, D.; Cornil, J.; Silbey, R.; Millié, P.; Brédas, J-L. *J. Chem. Phys.* **2000**, *112*, 4749. (c) Kistler, K. A.; Spano, F. C.; Matsika, S. *J. Phys. Chem. B* **2013**, *117*, 2032.
(37) Sheldrick, G. M. *Acta Crystallogr. A* **2008**, *64*, 112.
(38) Pascu, M.; Ruggi, A.; Scopelliti, R.; Severin, K. *Chem. Commun.* **2013**, *49*, 45.
(39) Rosa, J. C.; Galanakis, D.; Ganellin, C. R.; Dunn, P. M.; Jenkinson, D. H. *J. Med. Chem.* **1998**, *41*, 2.
(40) Rajakumar, P.; Padmanabhan, R. *Tetrahedron* **2011**, *67*, 9669.